Engineering Structures 213 (2020) 110547

Contents lists available at ScienceDirect

Engineering Structures

journal homepage: www.elsevier.com/locate/engstruct

Analytical prediction model for circular SMA-confined reinforced concrete columns

Khaled Abdelrahman*, Raafat El-Hacha[1]

Department of Civil Engineering, University of Calgary, Calgary, Alberta, Canada

ARTICLE INFO

Keywords:
Analytical
Axial
Confinement
Column
Model
Smart
Shape memory alloy
Wires

ABSTRACT

Several confinement methods using concrete casing, steel jacketing, and wrapping with Fibre Reinforced Polymer (FRP) sheets are widely implemented to enhance the strength and ductility of reinforced concrete (RC) columns. Recently, smart materials such as Shape Memory Alloys (SMA) are utilized for repair and strengthening of RC columns. The SMA's exhibit unique thermo-mechanical properties such as shape memory effect (SME) that enables the material to achieve high recovery stress (up to 600 MPa) and strain (up to 8%). Recent findings in the literature show the SME and high recovery stress of the SMA wires used to confine concrete columns significantly enhanced the strength and ductility performance of concrete. Realizing the potential of the SMA-confinement technique, this paper aims to present an analytical model to describe the behaviour of SMA-confined RC columns subjected to uni-axial compressive loads. Experimental data are compared against theoretically predicted results to validate the proposed analytical model. Results show the proposed analytical model predictions are in good agreement with the experimentally observed axial compressive response of SMA-confined RC columns.

1. Introduction

Structural engineers always seek for smart materials and innovative strengthening techniques to effectively and efficiently address the escalating deterioration of structures. Recent assessment reports found that 50% of bridges in Canada are over 60 years old, and most of these bridges are classified as structurally deficient and/or functionally obsolete [1]. The situation concerning Canada's Infrastructure is considerably worse. According to the Technology Road Map (TRM) consortium, about 28% of Canada's Infrastructure is more than 80 years old, with another 31% being between 40 and 80 years old. An estimated 79% of the infrastructure life expectancy has been already utilized [1]. In their study, Mirza and Ali [2] suggested that the average remaining service life of these infrastructure would be less than 20% by the year 2014.

The occurrence of national disasters such as earthquakes, specifically the 1971 San Fernando earthquake, the 1989 Loma Prieta earthquake, the 1994 Northridge earthquake, and the 1995 Kobe Japan earthquake demonstrate the vulnerability of our highly deteriorated infrastructure to ground motions [3]. Excessive investigations conducted on collapsed structures by earthquakes showed that the failure of one or more of the reinforced concrete (RC) columns led to the progressive failure of the structure. The failure of these RC columns was attributed to the poor quality of design and construction practices that led to inadequate flexural ductility and shear capacity to sustain the earthquake loadings.

The repair and rehabilitation of the present infrastructure, specifically column members, should be of high priority. The main focus should lie in reviving the deteriorating infrastructure to become structurally sound, safe, and durable. The traditional repair and rehabilitation methods involve confinement techniques using concrete casing or steel jackets. These traditional strengthening techniques possess inherent disadvantages due to the fact that the strengthening materials suffer from the same deterioration factors as the parent material. Thus, the use of durable (non-corrosive) and lightweight materials that exhibit high strength-to-weight ratio such as Fibre Reinforced Polymers (FRP) soon replaced conventional materials (concrete and steel) utilized for confinement strengthening methods.

The constant demand for innovative materials that are stronger, lighter, durable, and ductile with tailored properties depending on the nature of the application, has produced a new branch of materials termed shape memory alloys (SMA). These smart SMA materials offer numerous unique advantages making them a breakthrough innovation for the building industry applications, specifically, for confinement of concrete members. Research advancing towards utilizing SMA's as a confinement material could establish quick, effective, efficient, and durable repair and rehabilitation methods that could potentially be

* Corresponding author. Tel.: +1 403-472-7403.
E-mail addresses: kabdelra@ucalgary.ca (K. Abdelrahman), relhacha@ucalgary.ca (R. El-Hacha).
[1] Tel.: +1 403-220-4817.

https://doi.org/10.1016/j.engstruct.2020.110547
Received 9 September 2019; Received in revised form 11 February 2020; Accepted 17 March 2020

implemented to rectify Canada's deteriorating infrastructure.

Recent experimental research findings on SMA-confined concrete reported in the literature demonstrate the effectiveness of the SMA wires in increasing the strength and significantly enhancing the ductility of concrete [3–17]. These new materials have shown great potential to replace several confinement techniques such as concrete casing, steel jacketing, and FRP sheets. For industrial acceptance, structural design engineers require a reliable analytical model to predict the response of SMA-confined RC columns. Thus, the aim of this study is to present an analytical model that can predict the overall concentric axial stress-axial strain response of SMA-confined RC columns.

2. Background

Confinement methods can be categorized into two mechanisms: passive confinement or active confinement. Confining concrete through a passive confinement mechanism is the most commonly used strengthening technique for columns. A passive confinement system is unstressed at installation and only becomes activated when the concrete experiences significant transverse expansion at loads approaching the unconfined concrete compressive strength (Fig. 1). The passive confinement mechanism is directly related to the loading stages of the concrete column. At lower compressive loads, concrete is known to behave elastically and the transverse (hoop) strain is linearly related to the longitudinal strain by Poisson's ratio. At this stage, the concrete dilation is not sufficient to trigger the activation mechanism of the strengthening material (Fig. 1). As the load is increased, micro-cracks begin to coalesce forming macro-cracks that increase the transverse strain of the concrete. The strengthening material is then activated by resisting the concrete expansion through a confinement pressure forcing the concrete to be in a tri-axial state of stress (Fig. 2). This allows the concrete to sustain plastic deformations with axial strains and stresses higher than its unconfined failure values.

A less familiar approach to strengthening of concrete columns is through an active confinement mechanism. Research studies have shown that achieving active confinement of concrete columns using conventional materials such as concrete, steel, or FRP sheets were impractical, expensive and required excessive time, labour, and cost [18–20]. However, an active confinement mechanism has major advantages over the passive confinement mechanism. The active

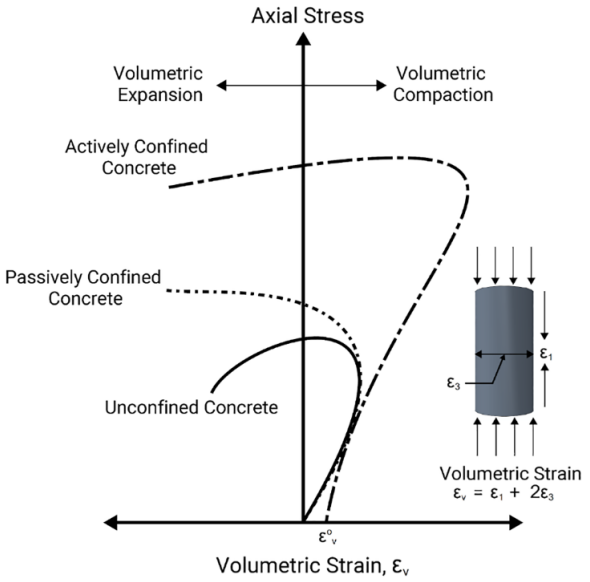

Fig. 1. Axial stress vs. volumetric strain response of unconfined concrete, passively confined concrete, and actively-confined concrete.

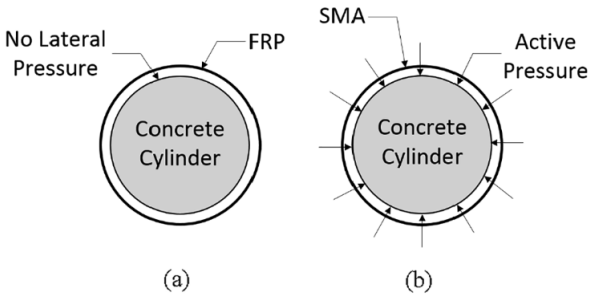

Fig. 2. (a) Passive confinement mechanism and (b) active confinement mechanism.

confinement pressure is independent of the lateral dilation of the concrete and is applied independently by the confinement material. This implies that the confining material is engaged prior to axial loads applied to the column (Fig. 1) and does not require the concrete to undergo any damage for the confining material to engage (Fig. 2). This ultimately results in a superior stress-strain response for actively confined concrete when compared to passively confined concrete.

The unique thermo-mechanical properties of the SMA can be utilized to actively confine concrete columns. SMA's are classified as smart materials and are recently utilized for strengthening and repairing of concrete structures. The most common form of SMA wires used for concrete confinement applications is Nickel-Titanium (*NiTi*) because it possesses unique thermo-mechanical properties such as the Shape Memory Effect (SME) along with high recovery stress (up to 600 MPa) and strain (up to 8%) [8]. The SMA's have two phases, a high temperature phase called austenite and a low temperature phase called martensite. The austenite phase is considered as the parent phase and the martensite phase as the product phase. The transformation from one phase to the other can occur by either applying an external stress or by changing the temperature. The forward transformation describes the transformation of the SMA from the austenite phase to the martensite phase, and the reverse transformation describes the transformation of the SMA from the martensite phase to the austenite phase. One of the unique thermo-mechanical properties of the SMA's is its capability to exhibit the shape memory effect (SME) phenomenon. The SME simply describes the forward and reverse transformations by changing the temperature of the SMA.

The SME of the SMA has been utilized to actively confine concrete columns. The confinement application usually involves wrapping pre-strained SMA wires around the circumference of the columns that are constrained at the ends of the concrete column. At this stage, the induction of heat will trigger the SME of the SMA wires and because of the constraint condition, a recovery stress is generated that actively confines the concrete. Experimental research investigations conducted in the literature reported enhanced load bearing capacity and ductility capacity in the performance of the SMA-confined concrete columns [3–17]. The performance of SMA-confined concrete cylinders has been also investigated numerically via Finite Element (FE) modeling [21–23]. However, there are limited analytical models in the literature to predict the response of SMA-confined concrete columns subjected to uniaxial compressive loading [24].

In light of the above-mentioned discussion, the objectives of this research study include the development of an analytical model to predict the axial stress- axial strain response of externally SMA-confined RC columns subjected to uni-axial compressive loading. This paper also presents the validation of the proposed analytical model by comparing the predicted results with the experimental results of unreinforced RC columns and SMA-confined RC columns.

3. Development of proposed analytical model

The objective of this section is to present the development of the analytical model for SMA confined RC columns subjected to concentric

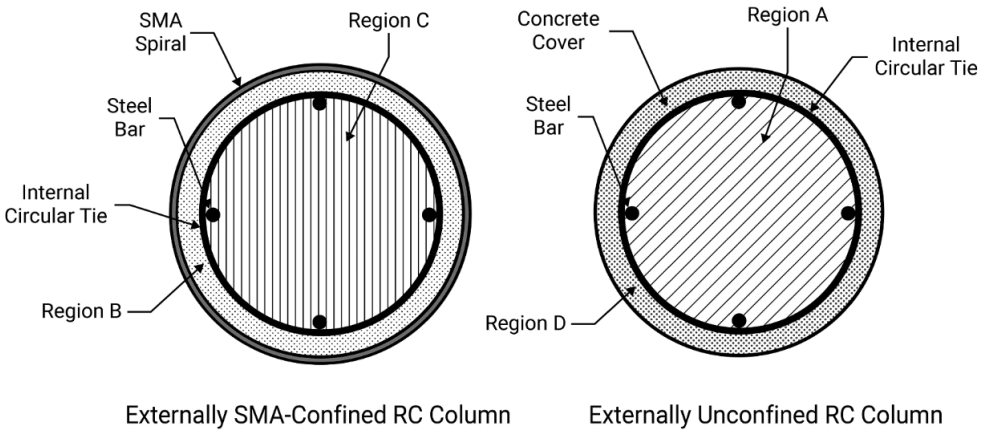

Fig. 3. Concrete region definition for externally confined RC column and externally unconfined RC column.

loading. The proposed analytical model incorporates the material constitutive models, namely the concrete, the reinforcing steel, and the SMA wires, as well as the interaction between them. This section also includes a proposed procedure to aid design engineers with the utilization of the proposed analytical model.

3.1. Fundamental material models

The proposed analytical model is based on fundamental material models, which describe the non-linear stress-strain relationships of the concrete, the internal steel reinforcement (longitudinal reinforcement and transverse circular ties), and the external SMA spirals. In this study, the effect of the lateral confinement applied by the internal circular ties and the external SMA spirals is incorporated directly into the stress-strain relationship of the concrete. The column cross-section can be divided into regions, where each region represents a unique confinement state of the concrete (Fig. 3). For each region, a concrete stress-strain response can be developed to account for the confinement state of its respective region. As shown in Fig. 3, Region A accounts for the response of concrete confined by internal circular ties; Region B accounts for the response of concrete confined by external SMA spirals, Region C accounts for the response of concrete confined by internal circular ties and external SMA spirals; and Region D accounts for the response of concrete without any internal or external confinement. The following sections presents the constitutive material model for concrete, as well as the stress-strain relationship for each confinement region. The constitutive material model for the steel reinforcement is also presented.

3.1.1. Concrete stress-strain response

The constitutive stress-strain material model for concrete was adopted from the model by Mander et al. [25], which was developed for concrete subjected to uniaxial compressive loading and confined by transverse reinforcement. The model is suitable for any concrete sections with either circular or spiral ties, or rectangular hoops with or without supplementary cross ties. For the purpose of this study, the equations related to circular cross-section with transverse confinement are presented.

The stress-strain model is illustrated in Fig. 4 and is based on the equation suggested by Popovics [26]. The fundamental material model described in Eqs. (1)–(9) is applicable to the four concrete regions (A, B, C and D) described earlier. The effect of the lateral confinement (internal circular ties and/or external SMA spirals) on the concrete stress-strain response is accounted for in the effective lateral confinement pressure (f'_l) parameter, which will be defined independently for each concrete region.

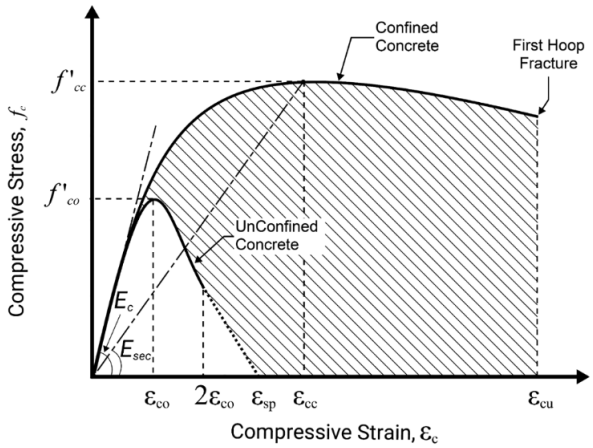

Fig. 4. Stress-strain model for monotonic loading of unconfined and confined concrete (after Mander et al. [25]).

For a slow (quasi-static) strain rate and monotonic loading, the longitudinal compressive concrete stress f_c is given by

$$f_c = \frac{f'_{cc}\ x\ r}{r - 1 + x^r} \tag{1}$$

where f'_{cc} is the compressive strength of confined concrete (defined later),

$$x = \frac{\varepsilon_c}{\varepsilon_{cc}} \tag{2}$$

where ε_c is the longitudinal compressive concrete strain and ε_{cc} is the longitudinal compressive concrete strain corresponding to the maximum concrete compressive stress (f'_{cc}), defined as

$$\varepsilon_{cc} = \varepsilon_{co}\left[1 + 5\left(\frac{f'_{cc}}{f'_{co}} - 1\right)\right] \tag{3}$$

where f'_{co} and ε_{co} are the unconfined concrete compressive strength and corresponding strain, respectively (generally $\varepsilon_{co} = 0.002$ can be assumed), and

$$r = \frac{E_c}{E_c - E_{\text{sec}}} \tag{4}$$

where E_c is the tangent modulus of elasticity of the concrete, defined as

$$E_c = 5000\sqrt{f'_{co}}\,MPa \tag{5}$$

The secant modulus of elasticity of the concrete E_{sec} is defined as

$$E_{\text{sec}} = \frac{f'_{cc}}{\varepsilon_{cc}} \tag{6}$$

The maximum confined concrete compressive strength f'_{cc} is calculated as

$$f'_{cc} = f'_{co}\left(-1.254 + 2.254\sqrt{1 + \frac{7.94f'_l}{f'_{co}}} - 2\frac{f'_l}{f'_{co}}\right) \tag{7}$$

where f'_l is the effective lateral confinement pressure calculated based on the defined concrete regions (A, B, C or D), as shown in Fig. 3.

The tensile behaviour of concrete is accounted for in accordance with CSA A23.3-14 [27], which defines the cracking strength of the concrete (f_{cr}) as

$$f_{cr} = 0.6\lambda\sqrt{f'_{co}} \tag{8}$$

where λ is the factor that accounts for the effect of low-density aggregates on the tensile strength. In this study, λ is taken as 1.0 for normal density concrete.

The cracking strength of the concrete (f_{cr}) is related to the cracking strain (ε_{cr}) through the following relationship

$$\varepsilon_{cr} = \frac{f_{cr}}{E_{co}} \tag{9}$$

It should be noted that in this study, tension stiffening is not accounted for after cracking of the unconfined concrete in tension.

3.1.2. Externally unconfined RC columns

The concrete stress-strain response of externally unconfined RC columns is comprised of two regions (Fig. 3); Region A represents a section of concrete with lateral confinement effects from the internal transverse circular steel ties, and Region D represents a section of concrete without any internal or external confinement.

For Region A, it is important to note that the maximum transverse pressure from the confining steel is only exerted effectively on that part of the concrete where the confining stress has fully developed due to the arching action. The arching action is assumed to occur midway between the levels of the transverse circular reinforcement (Fig. 5), where the area of the effectively confined concrete core A_e will be smallest and the area of the ineffectively confined concrete will be largest. In order to account for the arching action, an effective lateral confinement pressure for Region A is defined as

$$f'_{lA} = f_{lA}\, k_e \tag{10}$$

where f_{lA} is the lateral pressure from the transverse circular steel reinforcement and is assumed to be uniformly distributed over the surface of the concrete core.

The effective confinement coefficient is defined as

$$k_e = \frac{A_e}{A_{cc}} \tag{11}$$

where A_e is the area of the effectively confined core incorporating the arching action as a second-degree parabola with an initial tangent slope of 45°, calculated from Fig. 5 as

$$A_e = \frac{\pi}{4}\left(d_s - \frac{s'}{2}\right)^2 \tag{12}$$

The area of the concrete core (A_{cc}) is calculated as

$$A_{cc} = \frac{\pi}{4}d_s^2(1 - \rho_{cc}) \tag{13}$$

where d_s is the diameter of the circular ties between bar centres, s' is the clear vertical spacing between the circular ties, and ρ_{cc} is the ratio of the longitudinal reinforcement to area of core of section.

The lateral confining pressure (f_l) exerted by the circular steel ties is

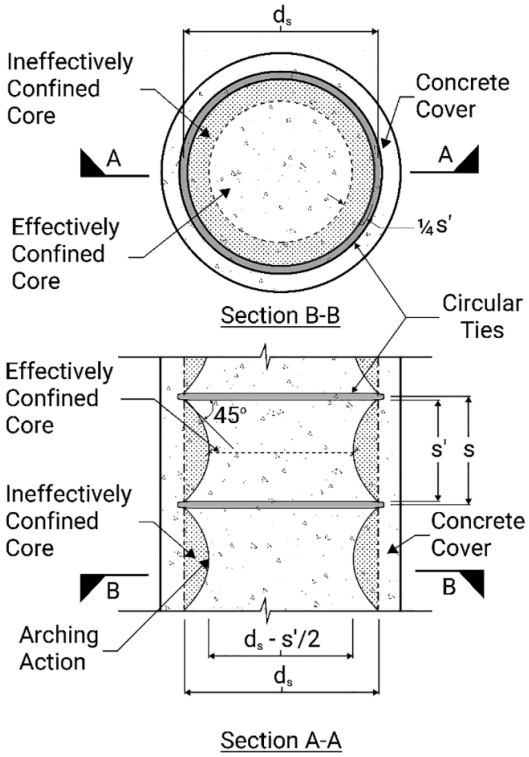

Fig. 5. Effectively confined core for circular hoop reinforcement (after Mander et al. [25]).

derived based on equilibrium of forces (Fig. 6) as

$$2f_{yh}A_{sp} = f_l s d_s \tag{14}$$

where f_{yh} and A_{sp} are the yield strength and cross-sectional area of the transverse tie reinforcement, and s is the centre-to-centre spacing of the circular tie.

The volumetric ratio (p_s) of the transverse circular tie reinforcement is defined as

$$\rho_s = \frac{A_{sp}\pi\, d_s}{\frac{\pi}{4}d_s^2 s} \tag{15}$$

Substituting Eq. (15) into Eq. (14) and rearranging gives

$$f_{lA} = \frac{1}{2}p_s f_{yh} \tag{16}$$

Therefore, the effective lateral confinement stress for Region A from Eq. (10) can be calculated as

$$f'_{lA} = \frac{1}{2}k_e\rho_s f_{yh} \tag{17}$$

The stress-strain response of Region D within the concrete cover of the column can be predicted using Eqs. (1)–(9). In these equations, the lateral confinement pressure (f'_{lD}) is set to zero (no confinement zone), and the decreasing branch in the region where $\varepsilon_c > 2\,\varepsilon_{co}$ is assumed to be a straight line reaching zero stress at the spalling strain ε_{sp} (Fig. 4).

The maximum longitudinal concrete compressive strain (ε_{cu}) of the externally unconfined RC columns is assumed to occur at the first hoop fracture and is predicted based on an energy balance approach. Ductile members are characterized by their prolonged load-deformation characteristics and their capability of dissipating significant quantities of strain energy prior to failure. Confined concrete columns exhibit additional ductility that can be considered to result from the additional strain energy stored by the transverse steel reinforcement. The

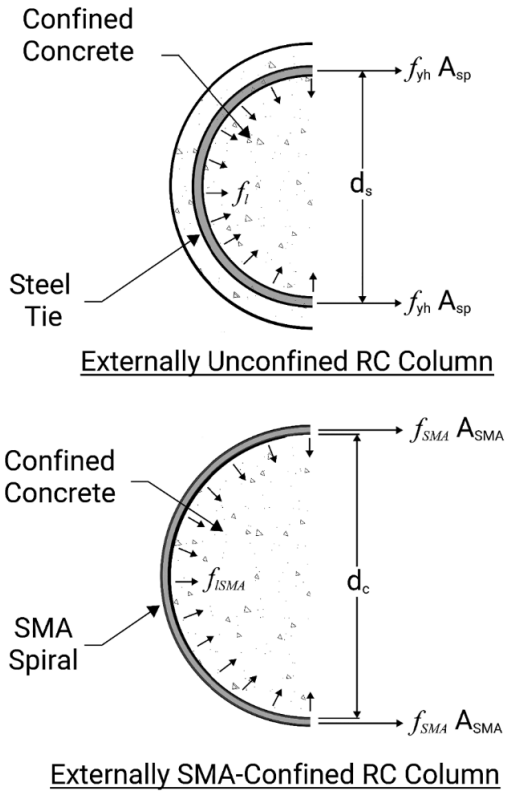

Fig. 6. Confinement forces for externally unconfined RC column and externally SMA-confined RC column.

additional internal strain energy of the transverse reinforcement (U_{sh}) can be quantified by the volumetric strain energy equation written as

$$U_{sh} = U_g - U_{co} \tag{18}$$

where U_g is the external work done on the columns to fracture the transverse reinforcement, and U_{co} is the work done to cause failure of an equivalent unconfined plain concrete column.

The external work done on the columns (U_g) is equal to the work done by the confined concrete core (U_{cc}) and the longitudinal steel (U_s), and substituting into Eq. (18) gives

$$U_{sh} = U_{cc} + U_s - U_{co} \tag{19}$$

The volumetric strain energy shown in Eq. (19) can be re-written as

$$\rho_s A_{cc} \int_0^{\varepsilon_{sf}} f_s d\varepsilon_s = \int_0^{\varepsilon_{cu}} A_{cc} f_c d\varepsilon_c + \int_0^{\varepsilon_{cu}} A_{sl} f_{sl} d\varepsilon_c - \int_0^{\varepsilon_{spall}} A_{cc} f_c d\varepsilon_c \tag{20}$$

where f_s and ε_s are the stress and strain in the transverse reinforcement, ε_{sf} is the fracture strain of the transverse reinforcement, f_c and ε_c are the longitudinal compressive stress and strain in the concrete, ε_{cu} is the ultimate longitudinal compressive strain in concrete, f_{sl} is the stress in the longitudinal reinforcement, and ε_{sp} is the spalling strain of unconfined concrete.

As suggested by Mander et al. [25], the first term on the left-hand side of Eq. (20) that corresponds to the total area under the stress-strain curve for the transverse reinforcement up to the fracture strain ε_{sf} can be approximated as

$$U_{sf} = \int_0^{\varepsilon_{sf}} f_s d\varepsilon_s = 110\ MJ/m^3 \quad (\pm 10\%) \tag{21}$$

The last term on the right-hand side of Eq. (20) that corresponds to the area under the stress-strain curve for the unconfined concrete can be approximated as

$$\int_0^{\varepsilon_{spall}} f_c d\varepsilon_c = 0.017\sqrt{f'_{co}} \quad MJ/m^3 \tag{22}$$

Thus, Eq. (20) simplifies to

$$110\rho_s A_{cc} = \int_0^{\varepsilon_{cu}} A_{cc} f_c d\varepsilon_c + \int_0^{\varepsilon_{cu}} A_{sl} f_{sl} d\varepsilon_c - 0.017 A_{cc}\sqrt{f'_{co}} \tag{23}$$

Eq. (23) can be solved numerically to determine the ultimate longitudinal concrete compressive strain (ε_{cu}) of the externally unconfined RC columns.

3.1.3. Externally SMA-confined RC columns

The constitutive concrete material model of the externally SMA confined RC columns is comprised of two regions (Fig. 3); Region B represents a section of concrete confined by the external SMA spirals, and Region C represents a section of concrete confined by the internal circular ties and the external SMA spirals. The only parameter in Eqs. (1)–(7) modified to predict the maximum SMA-confined concrete compressive strength (f'_{cc}) is the effective lateral confinement pressure (f'_l).

For Region B, the effective lateral confinement pressure (f'_{lB}) applied by the external SMA spirals is defined as

$$f'_{lB} = f_{lSMA} k_{eSMA} \tag{24}$$

where f_{lSMA} is the lateral pressure and k_{eSMA} is the effective confinement coefficient of the external SMA spirals.

The effective SMA confinement coefficient (k_{eSMA}) is calculated as

$$k_{eSMA} = \frac{A_{eSMA}}{A_c} \tag{25}$$

where A_c is the cross-sectional area of the concrete column.

The arching action for an externally SMA-confined RC column is assumed to occur mid-way between the levels of the SMA spirals as shown in Fig. 7. Thus, the area of the effectively SMA-confined concrete (A_{eSMA}) due to the arching action can be calculated as

$$A_{eSMA} = \frac{\pi}{4}\left(d_c - \frac{s'_{SMA}}{2}\right) \tag{26}$$

where d_c is the diameter of the concrete column and s'_{SMA} is the clear vertical spacing between the SMA spirals.

The lateral confining pressure (f_{lSMA}) exerted by the SMA spirals is derived based on equilibrium of forces (Fig. 6) as

$$2 f_{SMA} A_{SMA} = f_{lSMA} s_{SMA} d_c \tag{27}$$

where f_{SMA} and A_{SMA} are the tensile strength and the cross-sectional area of the SMA spirals, and s_{SMA} is the centre-to-centre spacing of the SMA spirals.

The volumetric ratio (ρ_{SMA}) of the external SMA spirals is defined as

$$\rho_{SMA} = \frac{A_{SMA}\ \pi\ d_c}{\frac{\pi}{4} d_c^2 s_{SMA}} \tag{28}$$

Substituting Eq. (28) into Eq. (27) and rearranging gives

$$f_{lSMA} = \frac{1}{2}\rho_{SMA} f_{SMA} \tag{29}$$

Therefore, the effective lateral confinement stress for Region B (f'_{lB}) from Eq. (24) can be calculated as

$$f'_{lB} = \frac{1}{2} k_{eSMA} \rho_{SMA} f_{SMA} \tag{30}$$

For Region C, the total effective lateral confinement stress applied by the internal circular ties and the external SMA spirals can be calculated as

$$f'_{lC} = f_l k_e + f_{lSMA} k_{eSMA} \tag{31}$$

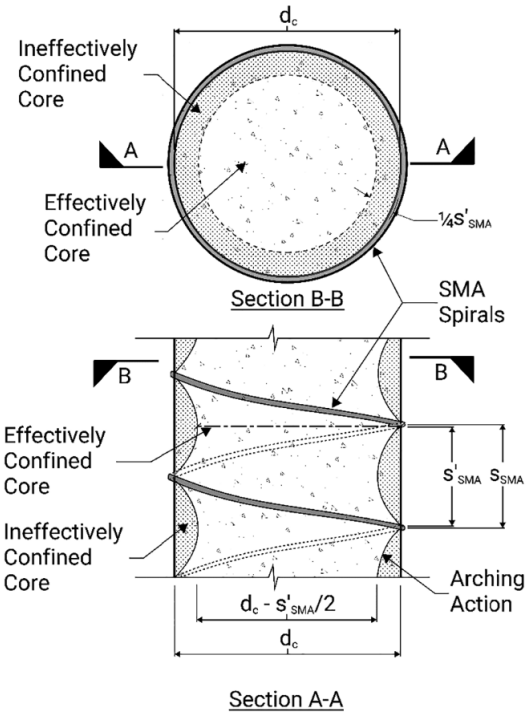

Fig. 7. Effective confinement of SMA-confined RC column (after Mander et al. [25]).

The effective lateral confinement stress for Region C can be also calculated as

$$f'_{lt} = \frac{1}{2}k_e\rho_s f_{yh} + \frac{1}{2}k_{eSMA}\rho_{SMA}f_{SMA} \tag{32}$$

Similarly, the maximum longitudinal concrete compressive strain (ε_{cu}) presented in Eq. (18) can be modified to account for the additional strain energy stored by the SMA spirals to predict the maximum longitudinal concrete compressive strain of the SMA-confined RC columns. The volumetric strain energy of the externally SMA-confined RC columns can be quantified by the following equation

$$U_{SMA} + U_{sh} = U_{cc} + U_s - U_{co} \tag{33}$$

The volumetric strain energy shown in Eq. (33) can be re-written as

$$\int_0^{\varepsilon_{SMA-f}} A_{SMA}f_{SMA}\,d\varepsilon_{SMA} + \rho_s A_{cc}\int_0^{\varepsilon_{sf}} f_s\,d\varepsilon_s = \int_0^{\varepsilon_{cu}} A_{cc}f_c\,d\varepsilon_c + \int_0^{\varepsilon_{cu}} A_{sl}f_{sl}\,d\varepsilon_c - \int_0^{\varepsilon_{spall}} A_{cc}f_c\,d\varepsilon_c \tag{34}$$

where, f_{SMA} and ε_{SMA} are the stress and strain in the SMA wires, respectively, and U_{SMA} is the total area under the tensile stress-strain curve for the SMA wires up to the fracture strain $\varepsilon_{SMA\text{-}f}$. Based on the mechanical properties and type of SMA wires adopted in this study, U_{SMA} can be approximated as

$$U_{SMA} = A_{SMA}\int_0^{\varepsilon_{SMA-f}} f_{SMA}\,d\varepsilon_{SMA} = 490\ \ MJ/m^3 \tag{35}$$

Thus, Eq. (34) simplifies to

$$490A_{SMA} + 110\rho_s A_{cc} = \int_0^{\varepsilon_{cu}} A_{cc}f_c\,d\varepsilon_c + \int_0^{\varepsilon_{cu}} A_{sl}f_{sl}\,d\varepsilon_c - 0.017A_{cc}\sqrt{f'_{co}} \tag{36}$$

Eq. (36) can be solved numerically to determine the ultimate longitudinal concrete compressive strain (ε_{cu}) of the externally SMA-confined RC columns.

The constitutive material properties of SMA was based on Nickel Titanium (*Ni-Ti*) SMA wires with a cross-sectional diameter of 1.9 mm. The *Ni-Ti* SMA wires were supplied by the manufacturer [28] in a pre-strained condition that could provide a linear strain recovery up to 6.3% when heated above the austenite finish temperature (As) of 60 °C. The constitutive material properties of the *Ni-Ti* SMA wires as reported by the manufacturer [28], had a mean ultimate tensile strength of 818 ± 50 MPa, a mean elastic modulus of 462 ± 5 MPa, and a strain at failure of 41 ± 5%. The maximum residual recovery stress of the *Ni-Ti* SMA wires to actively confine the concrete was 485 ± 1.6 MPa [29]. The experimental stress-strain response of the martensitic and austenitic *Ni-Ti* SMA wires adopted in this study is shown in Fig. 8. Further information about the characterization and the material properties of the SMA wires can be found in Abdelrahman [29].

3.1.4. Longitudinal steel reinforcing bars

The experimental results of the tensile tests conducted on the longitudinal steel reinforcement is shown in Fig. 8. A simplified bi-linear approximation provides an accurate representation of the stress-strain response of the reinforcing steel. The constitutive stress-strain model adopted in this study consisted of a linear elastic stress-strain response up to the yield point. Then, the stiffness of the reinforcing steel is reduced and is represented by a change in the slope of the stress-strain response. This phase consists of a linearly increasing behaviour until rupture of the reinforcing steel (Fig. 9). Further information about the characterization and the material properties of the reinforcing steel can be found in Abdelrahman [29].

3.2. Assumptions and limitations of proposed model

1. The analytical model is based on equilibrium of forces, strain compatibility, and plain sectional analysis;
2. The developed equations are appliable to concrete columns subjected to slow (quasi-static) strain rate and monotonic loading;
3. A confined and an unconfined concrete constitutive model is assumed for various regions within the cross-section of the concrete column;
4. Tension stiffening is not accounted for after cracking of the unconfined concrete in tension;
5. The constitutive material response of the reinforcing steel was assumed to exhibit a bi-linear response to failure;
6. The constitutive material response of SMA wires was for type *Ni-Ti* SMA with a distinctive curvi-linear stress-strain response;
7. A perfect-bond is assumed between the concrete and the internal steel reinforcement, and a perfect bond is assumed between the concrete and the external SMA wires.

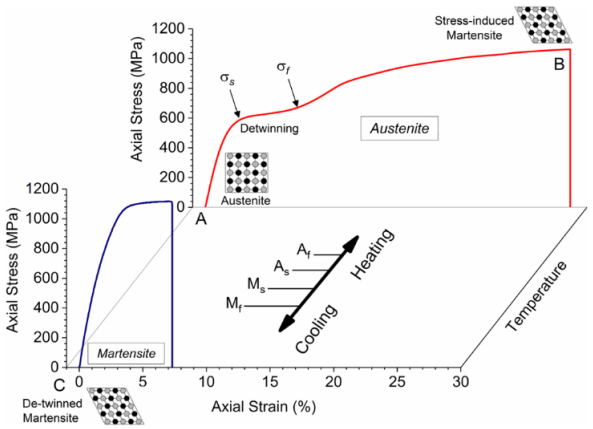

Fig. 8. Stress-strain behaviour of the SMA wires in the martensite and austenite phases.

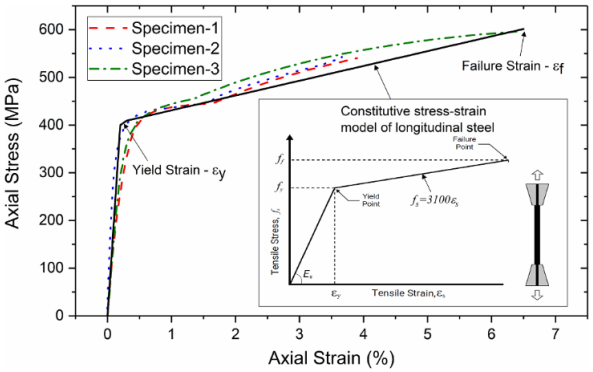

Fig. 9. Verification of the stress-strain model of the longitudinal steel.

8. The model is valid for concrete specimens with a maximum aspect ratio of 4, low-to- medium concrete strength columns, and externally confined with *Ni-Ti* SMA wires.

3.3. Procedure to utilize proposed analytical model

This section includes the procedure to utilize the developed analytical model to predict the concentric axial stress-axial strain response of unconfined RC column and externally SMA-confined RC columns. The procedure includes the following steps:

1. determine the constitutive material properties of concrete, longitudinal steel reinforcement, internal transverse circular steel tie and the external SMA spirals required to calculate the parameters used for Eq. (1);
2. Determine the effective lateral confinement pressure for the defined concrete regions of the externally unconfined RC column (Regions A and D) and the externally SMA-confined RC column (Regions B and C);
3. Insert the computed respective effective lateral confinement pressure for the defined regions (A, B, C, and D) of the concrete into Eq. (7);
4. At this stage, all the parameters required to formulate the stress equation (Eq. (1)) as a function of the input strain for the defined regions can be calculated;
5. The strain value is input into the formulated concrete stress-strain model and the longitudinal steel stress-strain model to determine the corresponding stress in each region of the concrete and the stress of the longitudinal steel reinforcement;
6. The total load resistance (P_i) of the RC column at that particular strain level can be calculated as follows:

$$P_i = f_{1i}A_{1i} + f_{2i}A_{2i} + f_{si}A_s \quad (37)$$

where f_{1i} and f_{2i} are the stress and their corresponding area (A_{1i} and A_{2i}) for Regions 1 and 2 (Regions 1 and 2 correspond to Regions A and D for externally unconfined RC column, and Regions B and C for externally SMA-confined RC column) of the concrete, respectively, and f_{si} and A_s are the stress and area of the longitudinal steel reinforcement;

7. The process as described above is repeated for increasing strain input values up to the calculated maximum longitudinal concrete compressive strain (ε_{cu}), to establish the concentric axial stress-axial strain response of the externally unconfined RC column or the externally SMA-confined RC column.

4. Validation of the developed analytical model and proposed procedures

It is imperative to verify the developed analytical model using Eqs. (1)–(9) and the proposed procedure to predict the concentric axial stress-axial strain response of the externally unconfined and the externally SMA-confined RC columns. The comparison between the predicted axial stress-axial strain response of the externally unconfined RC columns and the externally SMA-confined RC columns with the observed experimental behaviour is shown in Fig. 10 and Fig. 11, respectively.

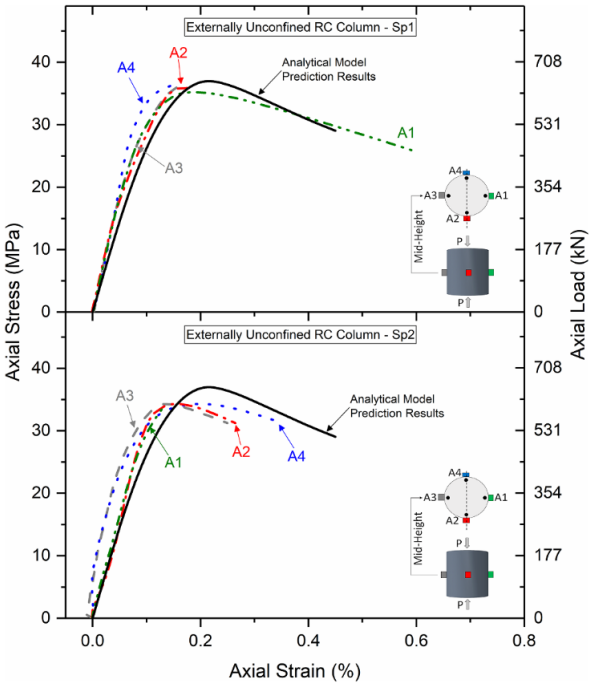

Fig. 10. Verification of the analytical model prediction results with the experimental data of the unconfined RC columns.

The experimental test program adopted for comparison purposes consisted of medium-scale, circular RC columns tested to failure under concentric uniaxial compressive load. The columns were 600 mm in height and 150 mm in diameter, and were internally reinforced with four 10 M steel bars and laterally reinforced with 6 mm circular steel ties at 100 mm on-centre. The SMA-confined RC columns were actively confined with *Ni-Ti* SMA wires at a pitch spacing of 10 mm. The specified concrete compressive strength of the specimens was 30 MPa, and the average yield strength of the 10 M longitudinal steel and the 6 mm diameter lateral steel was experimentally determined to be 404 MPa and 622 MPa, respectively. Further information with regards to the experimental testing and results of these columns can be found in Abdelrahman [29].

As shown in Fig. 10, the predicted results are compared with the results of two externally unconfined RC columns (Sp1 and Sp2). For each column, the axial strain results from four Pi-gauges mounted around the circumferential perimeter of the column is compared with the analytical prediction results. It can be clearly seen the prediction results using the proposed model were in good agreement with the experimental test results. The proposed analytical model captured the curvilinear behaviour of the axial stress-axial strain response exhibited by the externally unconfined RC columns. The maximum strength prediction from the analytical model was within 5% when compared to the strength capacity of the experimentally tested externally unconfined RC columns.

The Canadian design code CSA A23.3-14 [27] assumes that the maximum concrete strain at the extreme compression fibre to be 0.0035. The numerically determined ultimate axial concrete compressive strain of the externally unconfined-RC columns from Eq. (23) gives 0.0045. The higher strain value calculated is expected, since the proposed analytical model accounts for the effect of the transverse and longitudinal steel reinforcement.

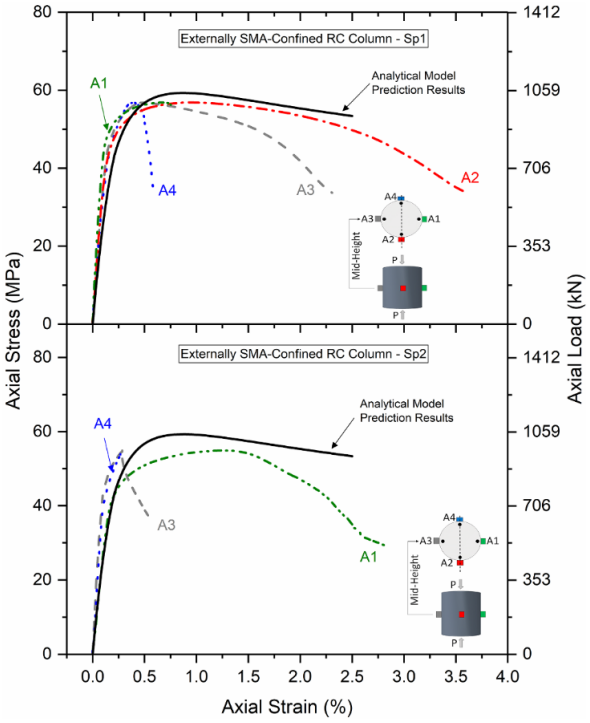

Fig. 11. Verification of the analytical model prediction results with the experimental data of the SMA-confined RC columns.

The data displayed in Fig. 11 show the predicted results from the proposed analytical model compared with the experimental results of two externally SMA-confined RC columns (Sp1 and Sp2). For each column, the axial strain results from four Pi-gauges mounted around the circumferential perimeter of the column is compared with the analytical prediction results. These results indicate that the analytical model prediction results compare well with the experimental data for the externally SMA-confined RC columns. The predicted maximum strength was within 6% when compared to the strength capacity of the experimentally tested externally SMA-confined RC columns. It is also apparent from Fig. 11 the predicted axial stress-axial strain response demonstrated a curvilinear behaviour similar to that observed from the experimental test results of the externally SMA-confined RC columns.

It is important to note that the accuracy of any strength prediction model for confined concrete depends on the ability of the model to accurately predict the axial strain value at the onset of failure. Several research studies employed a photogrammetric Digital Image Correlation (DIC) technique to investigate the axial strain variations across the surface of FRP-confined concrete column [30–37]. The DIC technique is capable of providing virtual strain measurements along the circumferential perimeter and height of the FRP-confined column. These studies showed significant axial strain variations (up to 50%) within the column, and between nominally identical sets of FRP strengthened columns. These findings agree well with the axial strain variations observed experimentally in the study reported in this thesis for the SMA-confined RC columns (Fig. 11). Literature on FRP-confined concrete columns reported that the axial strain variations are typically attributed to the dispersion of the aggregate particles along the diameter of the concrete column, the heterogenous nature of the concrete, the imperfections in the concrete surface from the formwork, and potential fibre breakage/misalignment during the production process of the FRP sheets. The latter is not applicable in the case of SMA-confined RC columns.

The average axial strain at ultimate (the average strain is calculated from four Pi-gauges located at the mid-height of the column) recorded experimentally from the externally SMA-confined RC columns Sp1 and Sp2 are 2.3% and 2.8%, respectively (Fig. 11). The numerically determined ultimate axial concrete compressive strain of the externally SMA-confined RC column subjected to concentric loading from Eq. (36) is calculated as 2.5%. Considering the inherent variability observed in the experimental ultimate axial strain of the tested specimens, the proposed analytical model predicts with reasonable accuracy the axial strain at ultimate for the externally SMA-confined RC columns.

5. Conclusions

Based on the investigations conducted in this study, the analytical model developed to predict the concentric axial stress-axial strain response showed good agreement with experimental test data of externally unconfined RC columns and the externally SMA-confined RC columns. The proposed model accurately predicted the maximum strength and ultimate strain values when compared to experimental data. Furthermore, the developed analytical model was able to capture the curvilinear response as exhibited experimentally for the unconfined RC columns and the externally SMA-confined RC columns.

For future research, the developed analytical model to predict the concentric response of SMA-confined RC columns can be utilized to predict the load (P) – moment (M) interaction response. It is crucial to understand and develop a P-M interaction response of SMA-confined RC columns, since almost all compression members in concrete structures are subjected to moments in addition to axial loads.

It is important to note that the interpretation and implementation of the results presented herein should be used with caution, as the analytical model is calibrated based on the SMA type adopted in this study. In addition, there is a critical need for further research to develop a comprehensive analytical model and design procedures that account for the effects of several parameters such as the column size, eccentric loading, and slenderness effects, to be readily available for design engineers to strengthen RC columns with active SMA-confinement. The research and adaptions of all aspects mentioned above is also required for square and rectangular RC columns confined with SMA wires.

The authors are currently in the works of developing an analytical model utilizing sectional analysis and layer-by-layer method to predict load-moment interaction response of SMA-confined RC columns. The analytical load-moment interaction model will be used to conduct a parametric study to better understand the effects of certain parameters, namely the concrete compressive strength, the SMA volumetric ratio, and the internal longitudinal steel reinforcement ratio on the axial load and bending moment response of SMA-confined RC columns.

Acknowledgments

The authors would like to express their gratitude to the University of Calgary as well as the Natural Sciences and Engineering Research Council of Canada (NSERC) for their financial support of this research project. The authors would also like to thank the technical staff at the University of Calgary for all of their expertise and help on this project.

References

[1] The Canadian Society of Civil Engineering. Civil infrastructure systems technology Roadmap 2003-2013; June 2003. 5pp.
[2] Mirza S, Ali MS. Canada's infrastructure crisis: where do we go from here?". In: Proceedings of the 7th international conference on FRP composites in civil engineering (CSCE 2014). Vancouver; 2014. 6pp.
[3] Andrawes B, Shin M, Wierschem N. Active confinement of reinforced concrete bridges using shape memory alloys. J Bridge Eng ASCE 2010;15(1):81–9.
[4] Abdelrahman K, El-Hacha R. Preliminary experimental investigation of SMA confined concrete. In: Proceedings of the International Conference on Concrete Repair, Rehabilitation and Retrofitting (ICCRRR). Leipzig; 2015. 8 pp.
[5] Abdelrahman K, El-Hacha R. Introduction to Shape Memory Alloys for concrete confinement applications. In: Proceedings of the fifth international workshop on performance, protection, & strengthening of structures under extreme loading (Protect 2015). Detroit; 2015. p. 374–81.

[6] Abdelrahman K, El-Hacha R. Confining RC columns subjected to concentric axial loading using Shape Memory Alloy wires. In: Proceedings of the third conference on smart monitoring assessment and rehabilitation of civil structures. Antalya; 2015: 8pp.
[7] Krustulovic-Opara N, Thiedmeman PD. Active confinement of concrete members with self-stressing composites. ACI Mater J 2000;93(3):297–308.
[8] Janke L, Czaderski C, Motavalli M, Ruth J. Applications of shape memory in civil engineering structures – overview, limits and new ideas. Mater Struct 2005;38(5):578–92.
[9] Choi Eunsoo, Nam Tae-hyun, Cho Sung-Chul, Chung Young-Soo, Park Taehyo. The behavior of concrete cylinders confined by shape memory alloy wires. Smart Mater Struct 2008;17(6):065032. https://doi.org/10.1088/0964-1726/17/6/065032.
[10] Choi E, Nam T-H, Yoon S-J, Cho S-K, Park J. Confining jackets for concrete cylinder using NiTiNb and NiTi shape memory alloys wires. Phys Scr T139 2010. 4pp.
[11] Destrebecq J-F, Balandraud X. Interaction between concrete cylinders and shape memory wires in the achievement of active confinement. Materials with complex behaviour. Adv Struct Mater 2010;6:19–34.
[12] Mirzaee Z, Moavalli M, Shekarchi M. Experimental investigation of compressive concrete elements confined with shape memory Ni-Ti wires. In: Proceedings of the fracture mechanics of concrete elements and concrete structures – assessment, durability, monitoring and retrofitting of concrete structures. Seoul; 2010. p. 1173–8.
[13] Shin M, Andrawes B. Experimental investigation of actively confined concrete using shape memory alloys. Eng Struct 2010;32(3):656–64.
[14] Zuboski GR. Stress-strain behaviour for actively confined concrete using shape memory alloys. MSc Thesis. USA: The Ohio State University; 2013. 213pp.
[15] Tran H, Balandraud X, Destrebecq JF. Improvement of the mechanical performance of concrete cylinders confined actively or passively by means of SMA wires. Elsevier Urban and Partner; 2014. 8pp.
[16] Buehler WJ, Gilfrich JV, Wiley RC. Effects of low-temperature phase changes on the mechanical properties of alloys near composition TiNi. J Appl Phys 1963;34:3232–9.
[17] Alam MS, Youssef MA, Nehdi M. Utilizing shape memory alloys to enhance the performance and safety of civil infrastructure: a review. Can J Civ Eng 2007;34(34):1075–86.
[18] Mortazavi A, Pilakoutas K, Son KSRC. column strengthening by lateral pre-tensioning of FRP. Constr Build Mater 2002;17(6–7):491–7.
[19] Yan Z, Pantelides CP, Reaveley LD. Seismic retrofit of bridge columns using fiber reinforced polymer composite shells and shape modification. In: Proceedings of the fourteen world conference on earthquake engineering. Beijing; 2008. 8pp.
[20] Reisi M, Mostofinejad D, Azizi N. M-P curves for strengthened concrete columns with active confinement. In: Proceedings of the fourteen world conference on earthquake engineering. Beijing; 2008. 8pp.
[21] Chen Q, Andrawes B. 3D finite element modeling to study the behavior of shape memory alloy confined concrete. In: Proceedings of the fifteen world conference on earthquake engineering (WCEE). Lisbon; 2012. 10 pp.
[22] Chen Q, Andrawes B. Finite element analysis of actively confined concrete using shape memory alloys. J Adv Concr Technol-Mater, Struct Environ 2014;12(12):520–34.
[23] Abdelrahman K, El-Hacha R. Finite element modeling of SMA confined concrete. In: Proceedings of the concrete innovations: research into practice (Concrete 2015). Melbourne; 2015. 8pp.
[24] Andrawes B, Shin M. Seismic retrofitting of bridge columns using shape memory alloys. In: Active and passive smart structures and integrated systems, proceedings of SPIE – international society for optics and photonics, vol. 6928, 69281K-doi:10.117/12.775480.
[25] Mander JB, Priestly MJN, Park R. Theoretical stress-strain model for confined concrete. J Struct Eng ASCE 1988;114(8):1804–26.
[26] Popovics S. Numerical approach to the full stress-strain curve of concrete. Cem Concr Res 1973;3(5):583–99.
[27] Canadian Standard Associations CSA. Design of concrete structures A23.3-14; 2014. Ontario, Canada.
[28] Memry. SEAS Group Company. In: http://www.memry.com/products-services/material/wire [retrieved on 15 January 2015].
[29] Abdelrahman K. Performance of eccentrically loaded reinforced concrete columns confined with Shape Memory Alloy wires. PhD Thesis. Calgary, Canada: Department of Civil Engineering, University of Calgary; 2017. 471pp.
[30] Abdelrahman K, El-Hacha R. Validation of digital image correlation technique on CFRP and SFRP wrapped cylinders subjected to freeze-thaw environmental exposure. In: Proceedings of the fourth international conference on durability and sustainability of Fibre Reinforced Polymer (FRP) composites for construction and rehabilitation (CDCC 2011). Quebec City; 2011. 8p.
[31] Abdelrahman K. Effectiveness of steel-fibre reinforced polymer for confining circular concrete columns. MSc Thesis. Calgary, Canada: Department of Civil Engineering, University of Calgary; 2011. 351pp.
[32] Abdelrahman K, El-Hacha R. Behaviour of large-scale concrete columns wrapped with CFRP and SFRP sheets. J Compos Constr ASCE 2012;16(4):430–9.
[33] Bisby L, Take W, Bolton M. Quantifying strain variation in FRP confined concrete using digital image analysis. In: Proceedings of the first Asia-Pacific conference on FRP in structures (APFIS 2007). Hong Kong, China; 2007. p. 599–604.
[34] Bisby L, Take W. Strain localisations in FRP confined concrete: new insights. Struct Build 2009;162(5):301–9.
[35] Bisby L, Stratford T. The ultimate condition of FRP confined concrete columns: new experimental observations & insight. In: Proceedings of the fifth international conference on FRP composites in civil engineering (CICE 2010). Beijing; 2010. p. 599–602.
[36] White D, Take A. Particle Image Velocimetry (PIV) Software for Use in Geotechnical Testing. CUED/D-SOILS/TR322 2002: 1-14.
[37] White D, Take W, Bolton M. Soil deformation measurement using Particle Image Velocity (PIV) and photogrammetry. Géotechnique 2003;53(7):619–63.